2010

Contact Angle Of A Nano-Drop On A Heterogeneous Surface

John Ritchie
Virginia Commonwealth University

CONTACT ANGLE OF A NANO-DROP ON A HETEROGENEOUS SURFACE

A thesis submitted in partial fulfillment of the requirements for the degree of Master of Science in Chemistry at Virginia Commonwealth University

by

John A. Ritchie
Master of Science in Chemistry
Virginia Commonwealth University
College of Humanities and Sciences
Department of Chemistry
2010

Director: Dr. Alenka Luzar, Professor of Chemistry
Department of Chemistry

Acknowledgment

Firstly, I offer my apologies and appreciations to my wife Harriet and two girls, Alexandria and Allyson, for their enduring sacrifices to our relationship during this time. I thank my father Joseph for nurturing my interests in science and my mother Ann for listening to me share. I admire Dr. Bratko's knowledge and patience, without which I would not have made my achievements. I am grateful to Dr. Luzar for accepting me into her group and providing an environment for me to complete my degree while maintaining my professional career. I would also like to thank the members of our group, Dr. Chris Dobb, Dr. Jihang Wang and Dr. Jamileh Seyed, for their contributions.

Table of Contents

List of Tables

List of Figures

Abstract

CONTACT ANGLE OF A NANO-DROP

ON A HETEROGENEOUS SURFACE

By John Andre Ritchie, Master of Science

A thesis submitted in partial fulfillment of the requirements for the degree of Master of Science at Virginia Commonwealth University

Virginia Commonwealth University, 2010

Major Director: Dr. Alenka Luzar, Professor of Chemistry

We examine the relation between contact angle of a nanodrop of water and the location of surface-water interaction energy at the perimeter and beneath the drop. Young's equations gives the relationship between surface tension, at the three phase solid liquid vapor interface, and contact angle on a homogeneous surface. Cassie and Baxter generalized this equation to heterogeneous surfaces implying that contact angle corresponds to the average properties of the surface under the drop. McCarthy and coworkers pointed out it is the nature of the substrate at droplet perimeter that controls

contact angle. And more recently, McHale in his theoretical derivation applies the Cassie-Baxter equation to the area at the drop's perimeter. For a nanodrop, the situation is further complicated by the finite range of water-substrate interactions making the definition of the perimeter region somewhat arbitrary. We simulate nanodroplets of water on graphene-like surfaces having hydrophobic and hydrophilic interaction energy at the perimeter and beneath the drop using molecular dynamics. The microscopic analogue of the contact angle was extracted from simulation trajectory data. We confirm the contact angle is exclusively related to the surface interaction energy in the region of the drop's perimeter. We test the role of finite range of substrate-water interaction when the area of a circular hydrophilic patch beneath the drop's core is incrementally expanded until the contact angle is equivalent to that on the pure hydrophilic surface. We identify a range of interaction corresponding to a considerable drop in θ when plotting contact angle as a function of patch size. We show the observed contact angle dependence on the size of the patch can be predicted by the Cassie-Baxter mixing relation when limited to the area within the interaction range from the drop's perimeter.

Chapter 1 Introduction

Understanding the behavior of water at the nanoscale is important to the development of nanofluidics for industry, medicine and science.[1] Modifications to surfaces imparting specific chemical and physical properties are important in the development of new technologies.[2] The design of new materials with surface heterogeneities can be assisted by predictions of wetting properties based on the knowledge about surface pattern and properties of pure ingredients. Specifically, in this work we consider surface heterogeneities whose sizes are comparable to the size of surface droplets. Experimentally, this situation has been tested on surfaces with macroscopic drops and surface patches.[3] The works of both McCarthy[4] and McHale[5] emphasize the importance of surface properties under the drop perimeter, rather than the whole wetted area. In the present study we consider the importance of surface properties in the region of the three phase contact line on a nanoscale. This approach tests generalizations of conventional surface thermodynamics to small length scale system relevant to nanofluidics and design of surface-patterned nanomaterial. We examine the differences that inevitably separate macroscopic and nanoscale systems, as a continuum picture holds only approximately at the nano and molecular levels. Our computer experiments test how water-substrate interaction beneath the drop's core or at its' perimeter determines the contact angle. Secondly, we examine changes in contact angle as a hydrophilic surface beneath the drop's core approaches and eventually exceeds the three phase contact line.

For a macroscopic drop, Young's equation relates the contact angle θ to the three interfacial free energies.[6]

$$\gamma_{SL} + \gamma_{LV}\cos\theta = \gamma_{SV} \qquad (1)$$

where γ_{SL}, γ_{LV}, and γ_{SV} are the surface free energies of the solid-liquid, the liquid-vapor and the solid-vapor interfaces. The contact angle, θ, is the angle the liquid makes with the solid substrate.

Cassie and Baxter generalized Young's equation to include composite surfaces where surface area fractions are related to the contact angle.[7]

$$\cos\theta_C = f_1\cos\theta_1 + f_2\cos\theta_2 \qquad (2)$$

The apparent contact angle θ_C is equal to sum of the fractions f_1 and f_2 multiplied by the cosine of the contact angle $\theta_{1,2}$ for each surface fraction. In predicting wetting or dewetting, the Cassie-Baxter equation implicitly presumes any heterogeneities to occur on length scales that are small compared to the size of the drop, thus there is no dependence on the drop location.[4,8] A recent publication proposed using the local form of the Cassie-Baxter equation where only the region covered by the three phase contact line is used in determining f_1 and f_2 in equation (2).[5] However, no equation of this proposed local form was presented.

In this study, we use molecular dynamics simulations to probe the role of heterogeneities comparable to the size of the nanodroplets. Molecular simulations provide an ideal

framework for studies of nanoscale systems which are not accessible to laboratory measurements. We consider model graphene-like surfaces with hydrophobic and hydrophilic domains. The origin of different hydrophilicites is the strength of substrate atoms interaction with water. We consider two interaction strengths denoted as Carbon-3 and Carbon-4. Their Lennard-Jones (LJ) parameters and water contact angles on surfaces of given types are given in Table 1.

We created nine surfaces, each surface with a different LJ interaction energy beneath the drop and at the perimeter. We used LJ surface interactions corresponding to a hydrophilic surface with a carbon-oxygen interaction energy ε_{CO} of 0.120 kcal/mol, a hydrophobic one with interaction energy ε_{CO} of 0.0599 kcal/mol, and mixed hydrophobic-hydrophilic interaction energies. To test the influence of the three phase contact line on the contact angle of our nanodrop, we kept ε_{CO} beneath the core constant while ε_{CO} at the perimeter was varied, and we kept ε_{CO} at the perimeter constant while the ε_{CO} beneath the drop's core was varied. The patch beneath the drop's core was rectangular in these simulations. Here we found that the surface interaction energy at the drop's perimeter determines the contact angle.

Having verified that the surface at the drop's perimeter determines contact angle, we turned to an investigation of the influence of the interaction range as the patch contour approaches the drop's three phase contact line. To this end we examine contact angle as a function of the radius of an expanding hydrophilic circular patch beneath the drop. Plotting contact angle as a function of patch radius we identify a threshold corresponding

to a considerable decrease in contact angle. In our molecular dynamics simulations we incrementally increased the radius of the circular hydrophilic patch beneath the drop until the contact angle converged to the value of our pure hydrophilic surface.

Molecular Kinetic Theory Model

At equilibrium our nanodrop is characterized by movement of water molecules across the three phase contact line in both directions. Metaphorically, the drop seems to breathe. Wetting or dewetting can be described as an imbalance in movement of water molecules across the contact line, and equilibrium can be described by a balance in these movements. The molecular kinetic model of wetting proposed by Blake and Haynes[910] is derived from Eyring's activated rate theory (transition state theory). For the nanodrop in our experiment, the statistical mechanics view of the activated rate theory for the transport of liquids[9], involves the expansion of our nanodrop where energy is needed to displace the three phase contact line.

The frequency of displacement at the three phase contact line is characterized by K and the length of average displacement is give by λ. At equilibrium, displacements across the three phase contact line in both directions are equal. K_+ is positive displacement and K- is negative displacement. At equilibrium, K_0 is equal to zero and overall displacement K = K_+ = K-. Wetting is a net positive displacement where K_+ is greater than K-. The energies of the two states K_+ and K- are E_+ and E- respectively. For a positive displacement, K_+, there is a decrease in E_+ and an increase in E-, and for a negative displacement, K-, there is an increase in E_+ and a decrease in E-.

K_+, the frequency of positive displacement in, unit reciprocal time, is given by

$$K_+ = \left(\frac{k_B T}{h}\right)\frac{Z^*}{Z_+}\exp\left(\frac{-E_+}{k_B T}\right) \quad (3)$$

K-, the frequency of negative displacement, in unit reciprocal time, is given by

$$K_- = \left(\frac{k_B T}{h}\right)\frac{Z^*}{Z_-}\exp\left(\frac{-E_-}{k_B T}\right) \quad (4)$$

where k_B is Boltzmann's constant, T is the temperature, h is Planck's constant. Z^*, Z_+ and Z- are the partition functions for the activated and initial states.

The work done in displacement is given by

$$W = \gamma_{LV}(\cos\theta_0 - \cos\theta) \quad (5)$$

where γ_{LV} is the liquid-vapor surface tension, θ is the dynamic contact angle and θ_0 is the equilibrium contact angle. The work done by displacement is considered anisotropic.

If the work per unit done by displacement is used only in raising or lowering E_+ and E- then

$$W = \Delta n \delta w \quad (6)$$

where Δn is the number of displacement sites and δw is the work done on each site. The net displacement rate becomes

$$K_{net} = 2K\sinh\left(\frac{W}{\Delta n k_b T}\right) \quad (7)$$

at equilibrium when K = K_+ = K-. The velocity of displacement at the three phase contact line is given by

$$v = K\lambda = 2K\lambda \sinh\left(\frac{W}{\Delta n k_b T}\right) \quad (8)$$

Wetting or dewetting becomes an imbalance in surface tension force expressed as, $\gamma_{LV}(\cos\theta_0 - \cos\theta)$.[10]

Gibbs Free Energy for Surface Tension

In a solution where a liquid comes in contact with a vapor there exists an interface composed of the liquid and vapor. The surface tension is the force exerted at the liquid vapor interface.6 The energy at the interface is considered excess energy compared with the energy of the two bulk phases. Thus internal energy at the interface, U^i, is given by

$$U^i = U - U^v - U^l \quad (9)$$

where U is the sum of energies of a system, U^v is the internal energy of the vapor phase, and U^l is the internal energy of the liquid phase.

Gibbs free energy is defined as

$$G = H - TS \quad (10)$$

where H is the enthalpy, T is the temperature, and S is the entropy of the system. Because the Gibbs free energy of the interface is considered excess energy with respect to the energy of the two bulk phases, the G of the interface is

$$G^i = H^i - TS^i \quad (11)$$

where the superscript i indicates the interface.

Mechanical work in a capillary system is done by a change in the volume of the two bulk phases or by a change in area at the interface. Mechanical work is given by

$$dW = -pdV + \gamma dA \quad (12)$$

where p is the pressure, dV is the volume change, γ is the surface tension at the interface, and dA is the change in the area of the interface. Pressure-volume work is negative because energy flows from the system to the surrounding.

The equation for the internal energy of the thermodynamic system is

$$dU = dQ + dW \quad (13)$$

where dQ is the heat received by the system in a reversible process. Substituting equation (12) into equation (13) gives

$$dU = dQ - pdV + \gamma dA \quad (14)$$

The thermodynamic definition of energy for a reversible process is

$$dS = \frac{dQ}{T} \quad (15)$$

where dS is the change in entropy, dQ is the change in heat for a reversible process and T is the temperature of the system. The change in internal energy becomes

$$dU = TdS - pdV + \gamma dA \quad (16)$$

The enthalpy expression for a change in system energy is

$$dH = dU + pdV + Vdp \quad (17)$$

where dU is the change in internal energy of the system, p is the pressure, and dV is the change in volume. Substituting equation (16) for dU in equation (17) gives

$$dH = TdS - pdV + pdV + Vdp + \gamma dA \quad (18)$$

$$dH = TdS + Vdp + \gamma dA \quad (19)$$

Substituting equation (19) into equation (10) gives

$$dG = TdS + Vdp + \gamma dA - TdS \quad (20)$$

$$dG = Vdp + \gamma dA \quad (21)$$

At constant temperature, pressure and molecule number the Gibbs free energy expression for surface tension is

$$\left(\frac{\partial G}{\partial A}\right)_{T,P,N} = \gamma \quad (22)$$

By equation (11) the Gibbs free energy expression for surface tension at the interface is

$$\left(\frac{\partial G^i}{\partial A}\right)_{T,P,N} = \gamma \quad (23)$$

Chapter 2 Methods and Models

Molecular Dynamics – Canonical Ensemble

Molecular dynamics uses Newtonian mechanics to model a physical system where the laws of classical mechanics are followed. In molecular dynamics, Newton's equations of motion are integrated over time. Given a set of initial coordinates and velocities the subsequent time evolution of coordinates is determined. Particles move and collide with other particles in the same manner they do in the physical domain. In a canonical ensemble where temperature, volume and the number of particles is constant (NVT), the probability density is the Boltzmann function $e^{(-H(\Gamma)/k_BT)}$ where H(Γ) is the Hamiltonian, and Γ is the set of positions and momenta, k_B is the Boltzmann's constant and T is the temperature in Kelvin. In this way molecular dynamics uses statistical mechanics where the system is represented by an average configuration which in turn is represented by a Gaussian distribution. Initial velocities are chosen randomly from a Gaussian distribution. Because trajectories in molecular dynamics must be averaged statistically, thermodynamic quantities need to be allowed to reach equilibrium prior to using the data for sampling.[11]

Nose Hoover Thermostat

In a system with a fixed number of particles, volume and potential energy, the Nose-Hoover thermostat introduces a scaling of velocities which acts as an exchange of heat between the simulated system and an external heat reservoir.[12] In our simulation we used the Nose-Hoover temperature thermostat to control our canonical ensemble. A

dampening constant is applied to relax the temperature of the system to the target temperature in the simulation by applying friction to slow translational motion during each time-step in the simulation. The Nose-Hoover thermostat performs time integration at constant NVT where velocities and positions are updated for each time-step.

Time Integration – The Verlet Algorithm

The Verlet algorithm is used to solve the equations of motions at each time step. Positions are provided both forwards and backwards in time. The Verlet algorithm is described by the following equation:

$$r(t+\Delta t) = 2r(t) - r(t-\Delta t) + \frac{F(t)}{m}\Delta t^2 \qquad (24)$$

where the new position of the particle $r(t+\Delta t)$ is computed from the current position *r(t)* based on acceleration $F(t)/m$ and positions $r(t-\Delta t)$ from the previous step. The length of the time step Δt is chosen to fit with the type of particle, motion and interactions simulated.[13]

Calculation of Force

Force is calculated between all particle pairs within a cut-off distance r_c. The force calculation with respects to the x, y, and z-components is

$$f_{x,y,z}(r) = -\frac{\partial u(r)}{dx} - \frac{\partial u(r)}{dy} - \frac{\partial u(r)}{dz} = \left(-\left(\frac{x}{r}\right)\left(\frac{\partial u(r)}{\partial (r)}\right) - \left(\frac{y}{r}\right)\left(\frac{\partial u(r)}{\partial (r)}\right) - \left(\frac{z}{r}\right)\left(\frac{\partial u(r)}{\partial (r)}\right)\right) \qquad (25)$$

where *u(r)* is the potential energy of a particle pair, and each pair is counted explicitly.[13]

Periodic Boundary Conditions

In a simulation under periodic boundary conditions (PBC) particles interact with other particles in the central simulation box and with their replicated image in other cell boxes. When a particle moves in the central box, its periodic image in neighboring boxes moves in the same way. When a particle leaves the central box, its periodic image enters through the opposite face. A useful way to visualize PBC is to take the central box and roll it into a doughnut shape.[14] A minimum image criterion is used in PBC conditions to select the closest image of particle j to interact with particle i. To use minimum image criteria, the simulation cell length must be equal to or greater than twice the interaction cut-off radius.

Ewald Sums

Coulomb interactions among partial charges on water molecules were treated by the use of Ewald summation. The method has been developed to mitigate finite size effects in Coulombic systems by using infinite periodic replication. Taking advantage of the system's periodicity, upon appropriate decomposition of charge distributions, summation over infinite number of terms in real space is replaced by a single term in Fourier space for each atomic charge. For most purposes, the results of the Ewald sum technique coincide with those obtained from extrapolation to very large systems.[13] In studies of finite-size nanodroplets, periodic replication is not necessary in principle; however, because of the rapid convergence of its real space part, Ewald summation represents a faster alternative to the straightforward use of non-truncated potentials among all charge-pairs in the system.[15]

To compute the Coulomb contribution to the potential energy of our N particle system we need to sum the charges on each particle across all periodic boundary conditions. These charges cannot be summed for long range interactions because the sum is not convergent. To make the sum of the charges convergent, we represent each charge as a Dirac δ function. Then we screen each charge by surrounding each δ function with a diffuse charge of equal magnitude and opposite sign. Only the fraction of charge that is not screened contributes to the Coulomb potential energy, and it quickly goes to zero with increasing distance. These screened charges are only a fraction of the total sum of charges. To compensate for the screening, a smooth periodic charge representing the original point charge is added. This compensating charge is a periodic Gaussian and is represented by a Fourier transform.[13]

The above process is better visualized when explained with convolution mathematics where two functions are folded across each other. More specifically, randomly placed delta functions, representing point charges, are convoluted with a Gaussian smoothing function. To visualize the target effect of replacing each point charge with an equivalent Gaussian distribution, the simulation is represented in one dimension with randomly spaced pulses across the cell of width L. A narrow Gaussian is placed somewhere within L, then reflected across the axis. The Gaussian is moved from right to left across the string of randomly spaced deltas to generate a resultant convolution as a third function, which results in a function with a Gaussian shape. This achieves the target effect of replacing each point charge with an equivalent Gaussian distribution. The Fourier transform of convolution is the multiplication of those functions' Fourier transforms. The

three terms in the above process, the screened point charges due to the compensating cloud, the spurious "self" charge, and the oppositely charged Gaussian, are summed to give the long range electrostatic potential energy:

$$U_{Coul} = \frac{1}{2V}\sum_{k\neq 0}\frac{4\pi}{k^2}\left|\rho(k)\right|^2 e^{(-k^2/4\alpha)} - (\alpha/\pi)^{1/2}\sum_{i=1}^{N} q_i^2 + \frac{1}{2}\sum_{i\neq 1}^{N}\frac{q_i q_j erfc(\sqrt{\alpha} r_{ij})}{r_{ij}} \qquad (26)$$

where, V is the volume, ***k*** is the lattice vector in Fourier space, ρ is the charge density, α is the convergence parameter which controls the relative weights of real space and reciprocal space sums, N is the number of particles, q_i and q_j are charges on particles i and j separated by a distance r_{ij}, and the erfc (complementary error) function represents the unscreened point charges. The four square diagram in Figure 1 below describes the methods used to sum the charges in the simulation box across the PBC.

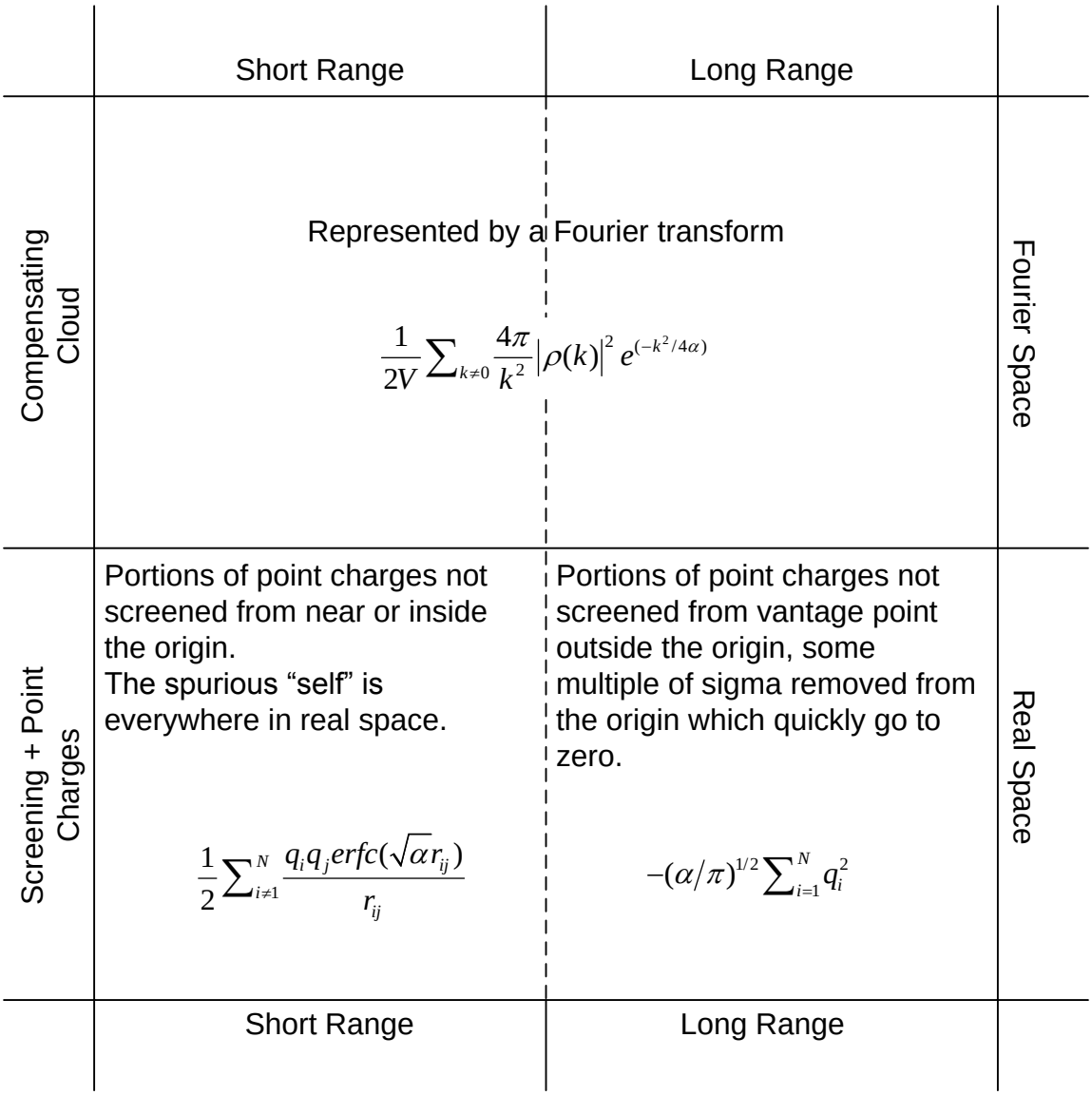

Figure 1: Four Square Diagram for the Method of Ewald Sums

The top two squares are the long and short range Coulomb potentials from the compensating cloud calculated in Fourier space. The bottom left square is the short range screening plus point charges summed in real space. For further detail and derivations, the reader is referred to references 13 and 14 in the Bibliography.

Water-Carbon Potential Model

The LJ 6-12 potential used to model interactions between the atoms in our molecular dynamics simulation is graphed in Figure 2 below. The LJ 6-12 potential is given by

$$V(r) = 4\varepsilon_{CO}\left[\left(\frac{\sigma_{CO}}{r}\right)^{12} - \left(\frac{\sigma_{CO}}{r}\right)^{6}\right] \tag{27}$$

where the pairwise potential V is a function of radius r, and σ_{CO} and ε_{CO} are the parameters for molecular separation distance at zero potential energy, and the depth of the energy well. We used the Simple Point Charge – Extended water model (SPC/E) in our molecular dynamics simulations. The SPC/E water model is a rigid three site model with each atom having a point charge.[16] Figure 3 is a ball and stick representation of the SPC/E model.

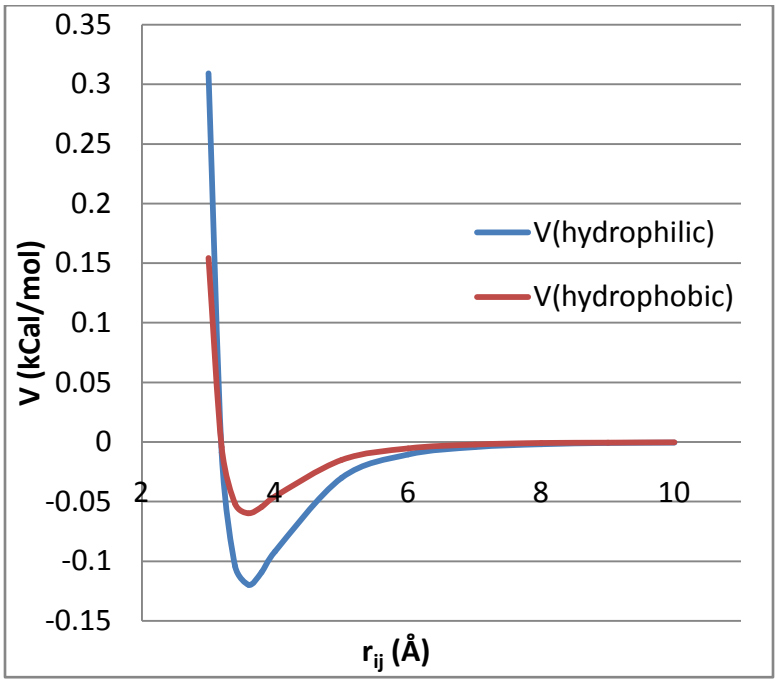

Figure 2: Lennard-Jones 6-12 Potential

Graph of the LJ 6-12 potential for interaction between the carbon atoms of the graphene-like substrate and the oxygen atoms of water. Table 1 lists the parameters used in the equation for the lines. The red line represents interaction between the hydrophobic substrate and water, and the blue line represents the interaction between the hydrophilic substrate and water.

Table 1 lists the essential parameters used in our simulation. The water-graphene interaction parameters were calculated using the geometric averages shown in the equations below,

$$\varepsilon_{CO} = (\varepsilon_{CC}\varepsilon_{OO})^{1/2} \quad (28)$$

$$\sigma_{CO} = (\sigma_{CC}\sigma_{OO})^{1/2} \quad (29)$$

where $\sigma_{CO,}$ σ_{CC}, and σ_{OO} are the carbon-oxygen, carbon-carbon, and oxygen-oxygen separation distance at minimum potential, and $\varepsilon_{CO,}$ ε_{CC}, and ε_{OO} are the LJ minimum potential energies.[8] The separation distance and minimum potential energies used in equations (28) and (29), and for simulation parameters are listed in Table 1.

Table 1: Simulation parameters

C-Atom	ε_{CO} (kcal/mol)	σ_{CO} (Å)	ε_{CC} (kcal/mol)	σ_{CC} (Å)	ε_{OO} (kcal/mol)	σ_{OO} (Å)
3	0.0599025517	3.19	0.0231060600	3.2144799121	0.1552976020	3.1655200897
4	0.1198051034	3.19	0.0924242398	3.2144799121	0.1552976020	3.1655200897

ε_{CO} is the carbon-oxygen LJ interaction energy. ε_{CC} is the carbon-carbon LJ interaction energy, and ε_{OO} is the oxygen-oxygen LJ interaction energy. σ_{CO} is the LJ separation distance for carbon-oxygen. σ_{CC} is the LJ separation distance for carbon-carbon, and σ_{OO} is the LJ separation distance for oxygen-oxygen.

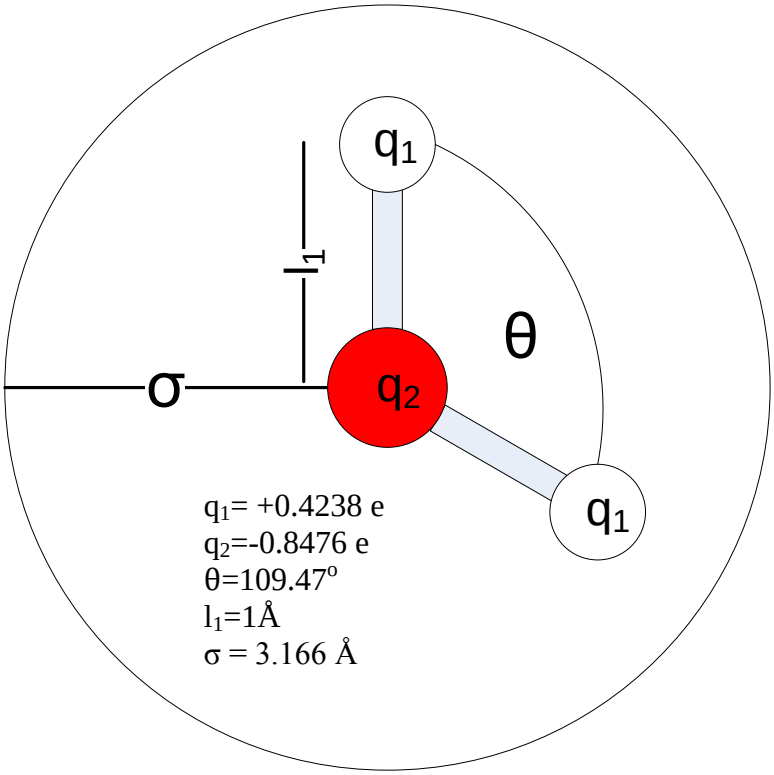

Figure 3: SPC/E Water Model

Ball and stick representation of the SPC/E water model.[16] θ is the angle between HOH. $q_1$and q_2 are the electronic charges on hydrogen and oxygen. σ is the separation distance between similar molecules at zero LJ potential energy. l_1 is the oxygen-hydrogen distance. A spherical cutoff of LJ interaction at r_c = 14 Å is applied.

Simulation Parameters

We used the 2009 code of Lammps (Large-scale Atomic/Molecular Massively Parallel Simulator) for our molecular dynamics simulations with the canonical NVT ensemble.[17] A Nose-Hoover thermostat was used to keep the temperature fixed at 300 K with a 100 fs damping relaxation time.[12] The water molecule bond length was constrained with the SHAKE algorithm, and graphene carbon positions were fixed. The LJ and Coulomb non-

bonded pair-wise interaction cutoff was set at 14 Å. We created a rectangular simulation box of dimensions Lx = 117.8 Å, Ly = 119.1 Å, and Lz = 300 Å, with periodic boundary conditions. The discrete positive nuclear charges on the carbon-like graphene patch beneath the drop spanned 23 Å by 25 Å.

We started with a 2000 molecule water drop pre-equilibrated at a hydrophilic surface, and a graphene surface consisting of 5,376 carbon-like atoms. Using the LJ parameters listed in the Table 1, we made seven pairs of surfaces, each with hydrophobic and hydrophilic regions approximately one fifth the contact surface area of the water drop. A pure hydrophobic and hydrophilic surface and a mixed hydrophobic-hydrophilic surface were also created.

Following an equilibration time of 200 ps, the last water drop trajectories were centered over the patch and the simulation was run for a time of 400 ps. Only those trajectories where the drop completely covered the patch were used in calculating the contact angle. If during the course of the simulation the water drop moved from over the patch, the last set of trajectories where the drop completely covered the patch were centered over the patch and the simulation was restarted. The random number for Gaussian distribution, used to represent the average configuration, was left unchanged. Four hundred trajectories were recorded from each simulation. Ten simulations were done for each of the nine surfaces.

To investigate the range of interaction between the solid substrate and the nanodrop at the three phase contact line, we created nine surfaces each consisting of a circular

hydrophilic patch beneath the drop surrounded by a hydrophobic surface. The hydrophilic patch radii used were 16.26, 17.4, 19.70, 20.85, 25.00, 30.00, 35.00, 40.00 and 45.00 Å. The water drop from the bottom row of Table 2 in Chapter 3 was used at the start of each 200 ps equilibration run. The same procedure described earlier was used here with the exception that only simulation trajectories where the drop's center of mass was within 4 Å of the patch center were used for our calculations.

Modeling the Heterogeneous Substrate

We used a graphene-like substrate, which is an allotrope of graphite having a single layer of carbon. The graphene-like structure is hexagonal with a carbon to carbon bond length of 1.418 Å and a bond angle of 120^{o}. To create the rectangular patch beneath the drop's core, we used AND, IF and TRUE logical statements to specify the carbon atom type for x-coordinates between 47 Å and 70 Å, and y-coordinates between 55 Å and 80 Å. The mathematical algorithms are given below

$$I2 = AND(x > 47, y > 55, x < 70, y < 80) \qquad (30)$$

$$C - Atom = IF(I2 = TRUE, 3, 4) \qquad (31)$$

where the AND logical returns a TRUE statement if the x and y-coordinates are within the specified range. The IF logical returns a carbon atom type 3 hydrophobic if I2 is TRUE, else a carbon atom is type 4 hydrophilic.

To create the circular patch beneath the drop, the IF logical was used to specify the carbon atom type by comparing a desired radius squared value with the radius squared

value of the carbon atom of the substrate. The radius squared value of the carbon atom coordinate is calculated by

$$r_i^2 = x_i^2 - 2x_i x_1 + x_1^2 + y_i^2 - 2y_i y_1 + y_1^2 \qquad (32)$$

where x_i and y_i are the x and y coordinates of the carbon atoms, and x_1 and y_1 are the coordinates for the center of the substrate. The IF logical was applied in the following equation

$$C - Atom = IF(r_i^2 < r^2, 4, 3) \qquad (33)$$

to specify a carbon atom type 4 hydrophilic if the radius squared of the carbon atom coordinates, r_i^2, is less than the desired radius squared of the hydrophilic patch, r^2, else a carbon atom type 3 hydrophobic.

Centering the Nanodrop

If during the course of the simulation the nanodrop strayed from over the patch, the simulation was stopped and the drop was centered over the patch. The nanodrop was centered by taking the last simulation trajectories where the nanodrop covered the patch, calculating the center of mass (COM), and shifting each atom's coordinates by the difference between the COM and substrate patch center. The COM for the x-coordinates of oxygen and hydrogen is given by

$$COMx_{i,j} = \frac{\sum_{i,j=1}^{N} (x_{i,j} m_{i,j})}{\sum_{i,j=1}^{N} m_{i,j}} \qquad (34)$$

where $x_{i,j}$ are the x coordinates trajectories, and $m_{i,j}$ are the masses of oxygen and hydrogen respectively.

The shift in the nanodrop's x-coordinates is given by

$$\Delta x_{i,j} = COMx_{i,j} - x_0 \qquad (35)$$

where x_o is the x-coordinate center over the patch.

The centered x-coordinate is given by

$$x'_{i,j} = x_{i,j} - \Delta x \qquad (36)$$

The y-coordinates are centered over the substrate patch using the same procedures as above.

Contact Angle

The contact angle is calculated from the best circular fit of a line drawn along the equimolar dividing surface of the drop's density profile using the method described by Werder et al.[8, 15,18] The equimolar dividing surface is where the density of the water drop decreases by 50 percent from the average. This dividing surface is found by sectioning the water drop into horizontal layers. Each layer is divided into radial bins where the density profile is measured. From this profile the equimolar dividing line is calculated. The contact angle as shown in Figure 4 is measured from this dividing line at a height of 3.19 Å above the graphene surface.

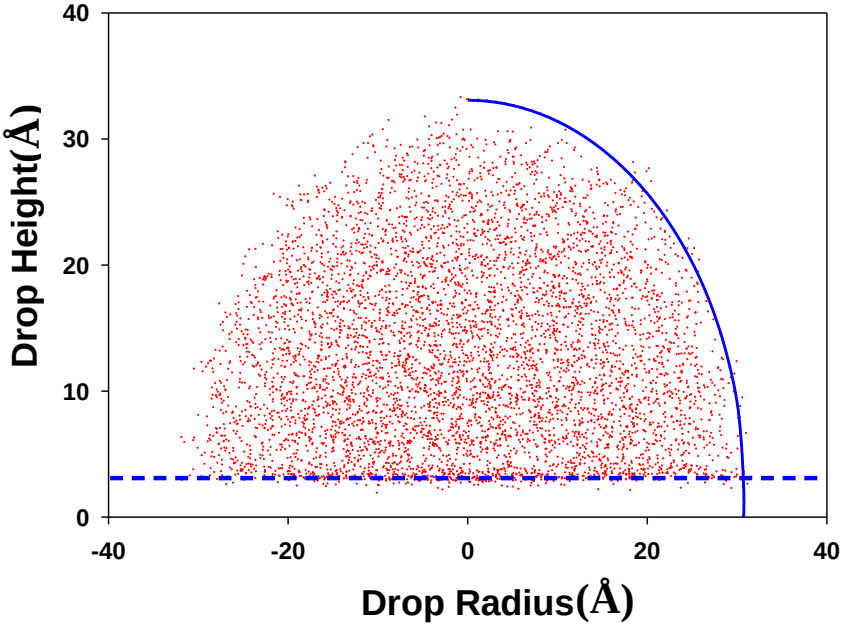

Figure 4: Contact Angle

Contact angle is the angle between the circular best fit of the drop's profile along the equimolar dividing surface (blue line), measured at the carbon-oxygen equilibrium distance of 3.19 Å (horizontal dash blue line).

Local Form of the Cassie-Baxter Equation

The local form of the Cassie-Baxter Equation is used to calculate the fractions f_1 and f_2 within the range of interaction of the drop's perimeter, as shown in Figure 5. The values of f_1 and f_2 substituted into Equation (2) are used to calculate the theoretical Cassie-Baxter contact angles for comparison against our experimental values shown in Figure 9.

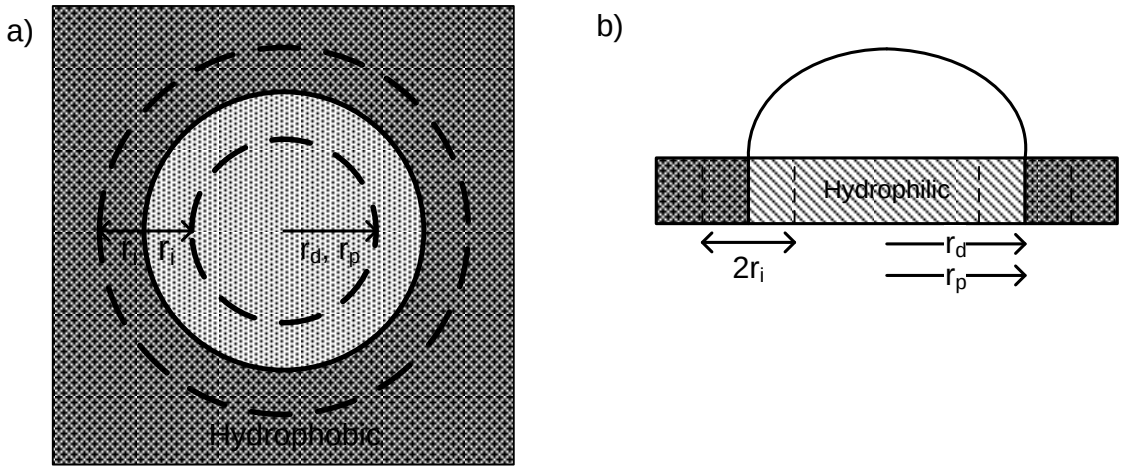

Figure 5: Local Form of the Cassie-Baxter Equation.

Schematic of our nanodrop on a heterogeneous substrate when the drop and patch radius are equal: a) planar, and b) cross sectional view. The radius of the drop is r_d, the hydrophilic patch radius is r_p, and the range of water-carbon interaction is r_i. Dashed lines frame the range of interaction.

The equations to calculate f_1 and f_2 are

$$f_1 = \frac{A_{pi}}{A_{ri}}, \text{ or} = 1 \text{ if } f_1 > 1 \qquad (37)$$

$$f_1 = 1 - f_1 \qquad (38)$$

$$A_{ri} = \pi(r_d + r_i)^2 - \pi(r_d - r_i)^2 \qquad (39)$$

$$A_{pi} = \pi(r_p)^2 - \pi(r_d - r_i)^2 \qquad (40)$$

where f_1 is the area fraction of the hydrophilic patch, A_{pi}, overlapping the area of the range of interaction, A_{ri}; and f_2 is the area fraction of the hydrophobic surface overlapping the area of the range of interaction. The radius of the nanodrop, circular patch, and range of interaction are r_d, r_p, and r_i respectively.

Chapter 3 Results

Results are presented, for our examination of water-substrate interaction beneath the drop's core versus at the three phase contact line in determining contact angle, in the subsection, Topology: Perimeter Versus Beneath the drop's Core. Results for our investigation of the influence of the interaction range as the patch contour approaches the drop's three phase contact line are presented under the subsection, Range of Interaction.

Topology: Perimeter Versus Beneath the Drop's Core

We find that the contact angle is exclusively related to the interaction energy at the drop's perimeter, or three phase contact line. Table 2 and Figure 6 show similar contact angles within each group despite varying the surface interaction energy beneath the drop. Simulations in group 1 each had equivalent hydrophilic surfaces at the drop's perimeter while the surface beneath the drop ranged from hydrophilic, mixed hydrophilic-hydrophobic and hydrophobic. The contact angles for group one are similar with angles of $65.0^{o} \pm 2.0^{o}$, $68.3^{o} \pm 2.2^{o}$ and $65.9^{o} \pm 1.1^{o}$. Simulations in group 2 had mixed hydrophobic-hydrophilic graphene-like surfaces at the drop's perimeter while the surface beneath the drop ranged from hydrophobic, hydrophilic and mixed hydrophobic-hydrophilic. The contact angles in group 2 are similar with angles of $92.2^{o} \pm 1.4^{o}$, $91.4^{o} \pm 1.4^{o}$ and $90.8^{o} \pm 1.6^{o}$. Simulations in group 3 had hydrophobic graphene-like surfaces at the drop's perimeter while the surface beneath the drop ranged from hydrophobic, mixed hydrophobic-hydrophilic and hydrophilic. The contact angles in group 3 were all similar, with angles of $115^{o} \pm 3^{o}$, $115^{o} \pm 3^{o}$ and $114^{o} \pm 2^{o}$.

Table 2: Surface interaction energy effect on contact angle

Group	ɵ(deg.)	ϵ_{CO} Under (kcal/mol)	ϵ_{CO} Perimeter (kcal/mol)
1	65.0 ±2.0	0.120	0.120
	68.3 ±2.2	0.0599/0.120	0.120
	65.9 ±1.1	0.0599	0.120
2	92.3 ±1.4	0.0599	0.0599/0.120
	91.4 ±1.4	0.120	0.0599/0.120
	90.8 ±1.6	0.0599/0.120	0.0599/0.120
3	115 ±3	0.0599	0.0599
	115 ±3	0.0599/0.120	0.0599
	114 ±2	0.120	0.0599

The table shows contact angles and standard deviations for simulations where the regions beneath the drops core and at the perimeter were varied. The contact angle, θ, is measured at 3.19 Å above the surface. ϵ_{CO} Under (kcal/mol) is the interaction energy between the carbon-like graphene surface beneath the drop's core and the oxygen atom of water. ϵ_{CO} Perimeter (kcal/mol) is the interaction energy at the three phase contact line. The hydrophilic interaction energy is 0.120 kcal/mol and the hydrophobic interaction energy is 0.0599 kcal/mol.

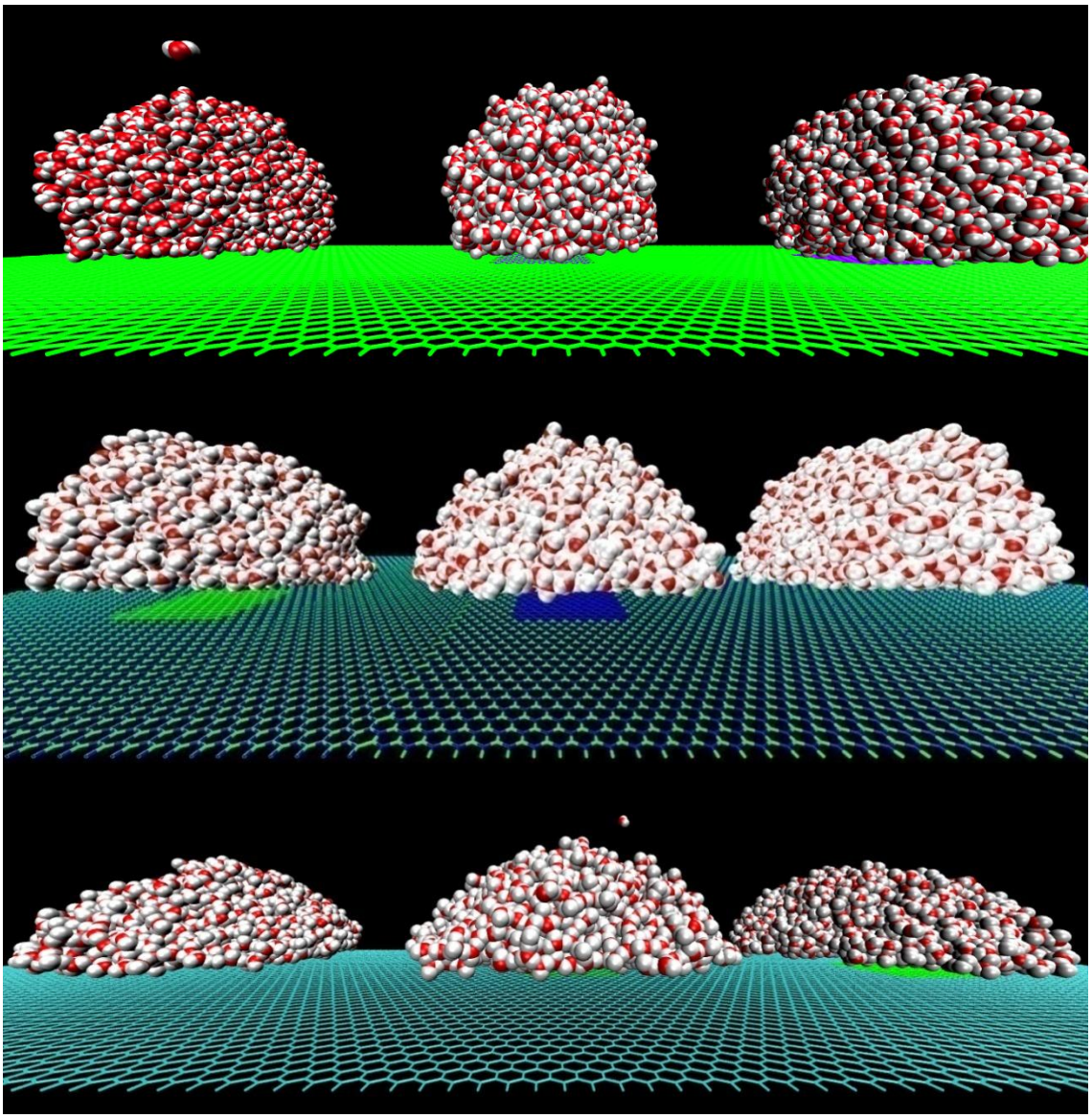

Figure 6: VMD Snapshots

Top row from left to right: The substrate beneath the drop's core is hydrophobic, mixed (hydrophobic-hydrophilic), and hydrophilic, while the substrate at the perimeter is hydrophobic for all. Middle row from left to right: The substrate beneath the drop's core is hydrophobic, hydrophilic, and mixed, while the substrate at the perimeter is mixed for all. Bottom row from left to right: The substrate beneath the drop's core is mixed, hydrophobic, and hydrophilic, while the substrate at the perimeter is hydrophilic for all.

Range of Interaction

Contact angles for our nanodrop as the radius of the hydrophilic substrate was expanded are presented in Table 3. On the pure hydrophobic surface (ε = 0.0599 kcal/mol) the contact angle was $115^{o} \pm 3^{o}$. No change in contact angle was observed for our nanodrop when the hydrophilic patch was introduced with an initial radius of 16.26 Å. The contact angle was $115^{o} \pm 3^{o}$, and the three phase contact line was a distance of 7.56 Å $\pm$1.02 Å from the 16.26 Å radius hydrophilic patch. The distance from the three phase contact line to the hydrophilic patch is shown in Table 3 in the Δr column. Initially, small increases in the hydrophilic patch radius were done to identify the point where water molecules at the perimeter begin to feel the approaching hydrophilic patch. A receding contact angle was measured with each further increase in the radius of the hydrophilic patch. The contact angle was measured as $90^{o} \pm 2^{o}$ when the radius of both the hydrophilic patch and nanodrop were 30 Å. Further increases in the radius of the hydrophilic patch show the nanodrop perimeter trailing the hydrophilic patch. For instance, when the radius of the patch was 35 Å the drop radius was 33.14 Å $\pm$0.34 Å and the contact angle was $77^{o} \pm 1$. Visual Molecular Dynamics[19] snapshots of our nanodrop as the radius of the hydrophilic patch was expanded are shown in Figure 7. This behavior is rationalized in terms of local mixing, discussed in Equations (37) through (40), according to the local Cassie-Baxter equation, within a nanoscale distance from the border of the patch, contact angle continuously decreases with the distance from the border until the distance is beyond the interaction range between water and substrate

atoms. We ended our simulations with a patch radius of 45 Å when the nanodrop contact angle was $68^{o} \pm 2^{o}$ and 8.84 Å ±0.50 Å from the inside of the hydrophilic patch.

Table 3. Interaction range of the circular patch

r_p (Å)	r_d (Å)	θ (deg.)	Δr (Å)
0	23.77 ±0.79	115 ±3	26.50
16.26	23.82 ±1.01	115 ±3	7.56 ±1.02
17.40	24.23 ±1.48	114 ±4	6.83 ±1.48
18.55	24.73 ±1.20	112 ±3	6.18 ±1.20
19.70	24.79 ±1.26	111 ±4	5.09 ±1.26
20.85	26.24 ±0.52	107 ±2	5.39 ±0.52
25.00	26.25 ±0.41	103 ±1	1.25 ±0.42
30.00	30.31 ±0.62	90 ±2	0.31 ±0.62
35.00	33.14 ±0.34	77 ±1	-1.86 ±0.33
40.00	35.29 ±1.07	69 ±2	-4.71 ±1.07
45.00	35.91 ±0.50	68 ±2	-8.84 ±0.50
∞	39.36 ±0.03	65 ±2	∞

The table shows contact angles, and standard deviations, for simulations examining the range of interaction at the perimeter. r_p is the radius of the hydrophilic patch beneath the water drop. r_d is the radius of the water drop. θ is the contact angle. Δr is the difference between the radius of the patch and the drop. The standard deviation is reported for the r_d, θ, and Δr.

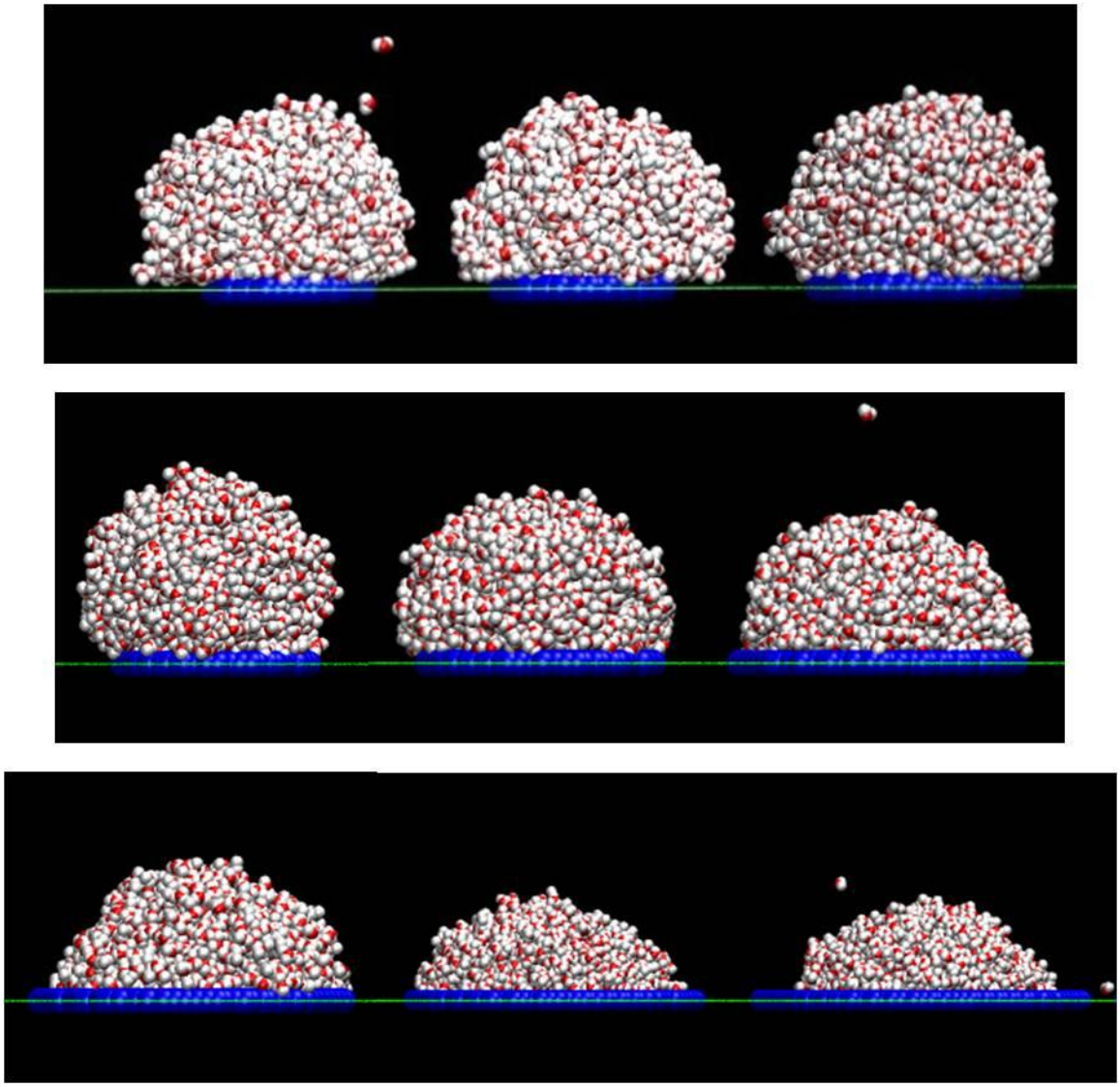

Figure 7: VMD Snapshots

Snapshots of 2000 water molecule droplets on graphene-like solid substrate with expanding hydrophilic substrate. Hydrophilic substrate of radius 16.26, 17.4, 19.70, 20.85, 25.00, 30.00, 35.00, 40.00 and 45.00 Å, surrounded by hydrophobic substrate (arranged from left to right, top to bottom). The hydrophilic substrate is rendered in Van der Waals mode for clarity.

Chapter 4 Discussion

A comparison of the effects of surface interaction energy in the regions beneath and at the perimeter of our nanodrop indicates the contact angle is related to substrate properties under the perimeter. Expanding the radius of the hydrophilic substrate beneath the drop causes a decrease in the contact angle as the perimeter of the drop is approached. The finite range of interaction is manifested as the hydrophilic substrate approaches the three phase contact line referred to as the *range of interaction*. The water molecules at the perimeter begin to interact with the hydrophilic patch indicated by a receding contact angle or wetting of the surface.

Three Phase Contact Line

Each data point in Figure 8 is the equilibrium contact angle associated with a hydrophilic circular patch of a specific radius. Figure 7 and Figure 8 shows the receding contact angle our nanodrop makes with each increase in the radius of the hydrophilic patch beneath the drop. The drop's contact angle is equal to the angle on a pure hydrophobic surface when the hydrophilic patch radius is less than 17.4 Å. The nanodrop entered a range of interaction from 17.4 Å to 40 Å. This range of interaction is the finite distance, between the substrate and interfacial water molecules at the perimeter, where the interaction energy affects contact angle. Beyond 40 Å the contact angle fully converged to the contact angle on a pure hydrophilic surface.

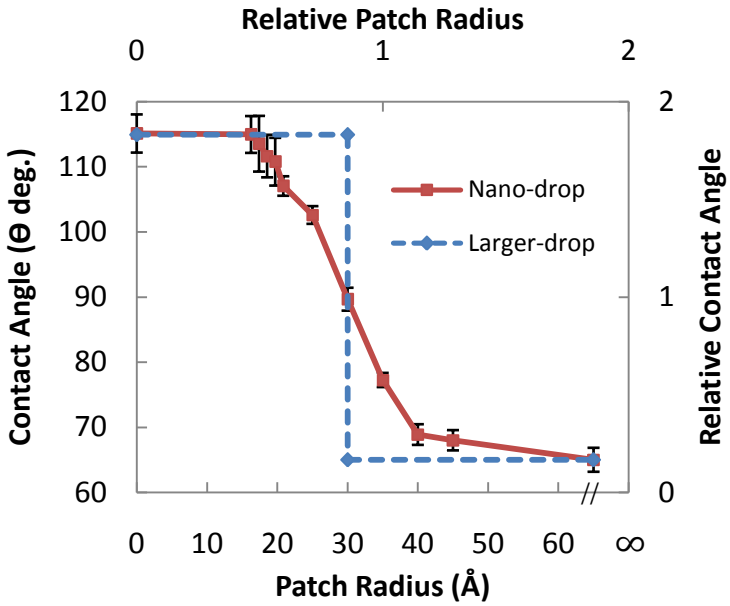

Figure 8: Transition from hydrophobic to hydrophilic substrate

The distance range exhibiting a decrease in water contact angle, with error bars, as the patch beneath the drop is expanded towards the perimeter is shown in Figure 8 (solid red). A similar transition range exists in macroscopic scenario. However the width is negligible in comparison to the size of macroscopic drop. Hence, the contact angle change appears to be a step function (dashed blue and secondary axis).

Fluctuations in Droplet Shape

In our simulations, we are able to observe the range of interaction shown in Figure 8 because of the law of large numbers in statistical mechanics, which predicts fluctuations in contact angle relative to the mean in a macrodrop decrease by a factor of $1/\sqrt{n}$, where n is the number of water molecules.[20] Compared to macroscopic drops, fluctuations are not negligible compared to the total drop size. The number of molecules in our Nanodrop is small compared to a macrodrop used by experimentalists. On a macroscopic scale,

fluctuations would be bigger in absolute magnitude, but negligible at the scale of the drop. Consequently, the contact angle would appear to decrease sharply, as sketched in Figure 8.

Observations of the time step trajectories at equilibrium with VMD show fluctuations into and out of the three phase contact line. Metaphorically the drop is breathing. This is explained by Blake in his molecular kinetic theory as a balance in net flux into and out of the liquid layer at the three phase contact line.[10] At any of the given 400 time steps in our simulations, the displacements are either wetting or dewetting and thus the three phase contact line fluctuates throughout the simulation at equilibrium.

Previous experimental work on heterogeneous surfaces shows abrupt contact angle changes as droplet size matched the size of surface patch. There is an apparent qualitative difference between these macroscopic observations and our nanodrop simulation. Extrand conducted a series of experiments measuring the contact angle on a heterogeneous surface where a drop was placed on a circular hydrophobic patch with a hydrophilic surface at the periphery.[3] A volume of liquid was added to advance the contact line. When the drop advanced onto the periphery, the contact line quickly advanced and the contact angle receded to the contact angle imparted by a pure surface of the periphery.[3]

Relevance to Cassie-Baxter Equation

Previous experimental work done by McCarthy, demonstrating work similar to this paper, except McCarthy used a macrodrop instead of a nanodrop, show no similarities in

contact angle when compared with the expected values from the Cassie-Baxter equation.[7] McHale's review of the theoretical basis of the Cassie-Baxter equation states if the single defect is local to the drop, as in McCarthy's work, the equation applies to the region at the perimeter.[5] McHale further states the local form of the Cassie-Baxter equation should be used for isolated drops on an isolated surface.[5] We use the range of interaction provided by the data in Table 3 and Figure 9 for surface fractions in our local form of the Cassie-Baxter equation. In the region of the graph in Figure 9 where the contact angle begins to recede, the data in Table 3 show the hydrophilic patch was a distance of 7.56 Å from the drop's perimeter. We identify this distance as the radius of the range of interaction, where the interfacial water molecules at the perimeter begin to interact with the hydrophilic substrate causing the contact angle to recede. In equations (39) and (40) the radius of the range of interaction, r_i, becomes 7.56 Å allowing us to calculate surface fractions, f_1 and f_2 for our local form of the Cassie-Baxter equation. Figure 9 shows good agreement between contact angles compared with calculated values from the local Cassie-Baxter equation.

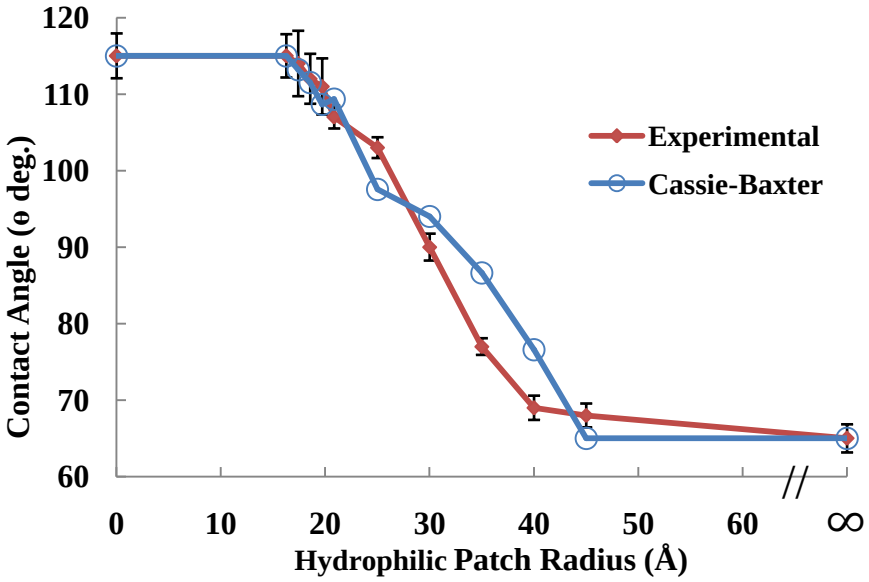

Figure 9: Experimental versus Cassie-Baxter

Experimental contact angles, with error bars, of our nanodrop compared with the calculated local form of the Cassie-Baxter equation, as the radius of the hydrophilic patch is increased. From a hydrophilic patch radius of approximately 16.26 Å to 40 Å the drop's contact angle recedes from 115^{o} to 65^{o}.

When we varied the surface interaction energies at the perimeter versus beneath the drop's core, we identified the perimeter region as determining contact angle. Secondly, we identified at what distance from the three phase contact line θ begins to be affected by the nature of the surface beneath the drop's core by expanding the radius of a hydrophilic circular patch until the contact angle was the same as on a pure hydrophilic surface. In doing so we identified a range of interaction observable only in a nanodrop simulation. In addition we observed equilibrium net flux of water molecules across the three phase contact line. Applying the range of interaction we were able to validate the local form of the Cassie-Baxter equation for our nanodrop.

Bibliography

1. Cheng, Y. K.; Rossky, P. J. Surface topography dependence of biomolecular hydrophobic hydration. *Nature* **1998,** *392* (6677), 696-699.
2. McHale, G.; Shirtcliffe, N. J.; Newton, M. I. Super-hydrophobic and super-wetting surfaces: Analytical potential? *Analyst* **2004,** *129* (4), 284-287.
3. Extrand, C. W. Contact Angles and Hysteresis on Surfaces with Chemically Heterogeneous Islands. *Langmuir* **2003,** *19* (9), 3793-3796.
4. Gao, L.; McCarthy, T. J. How Wenzel and Cassie were wrong. *Langmuir* **2007,** *23* (7), 3762-3765.
5. McHale, G. Cassie and Wenzel: Were They Really So Wrong? *Langmuir* **2007,** *23* (15), 8200-8205.
6. Young, T. An Essay on the Cohesion of Fluids. *Philos. Trans. R. Soc. London* **1805,** *95* (65), 65-87.
7. Cassie, A. B.; Baxter, S. Wettability of Porous Surfaces. *Trans. Faraday Soc.* **1944,** *40*, 546-551.
8. Werder, T.; Walther, J. H.; Jaffe, R. L.; Halicioglu, T.; Koumoutsakos, P. On the Water-Carbon Interaction for Use in Molecular Dynamics Simulations of Graphite and Carbon Nanotubes. *J. Phys. Chem. B* **2003,** *107* (6), 1345-1352.
9. Blake, T. D.; Haynes, J. M. Kinetics of Liquid/Liquid Displacement. *J. Colloid Interface Sci.* **1969,** *30* (3), 421-423.
10. Blake, T. D.; Clarke, A. Contact Angle Relaxation during Droplet Spreading: Comparison between Molecular Kinetic Theory and Molecular Dynamics. *Langmuir* **1997,** *13* (7), 2164-2166.
11. Ercolessi, F. Spring College In Computational Physics, 1997. Archiev retrieving system. www.ictp.trieste.it/www_users/calendar/cal1997.html (accessed October 30, 2010).
12. Nose, S. A molecular dynamics method for simulation in the canonical ensemble. *Molecular Physics* **1984,** *52* (2), 255-268.
13. Frenkel, D.; Smit, B. *Understanding Molecular Simulation From Algorithms to Applications,* 2nd ed.; Academic Press: San Diego, 2002; Vol. 1.
14. Allen, M. P.; Tildesley, D. J. *Computer Simulation of Liquids;* Oxford University Press: New York, 1991.
15. Daub, C. D.; Wang, J.; Kudesia, S.; Bratko, D.; Luzar, A. The influence of molecular-scale roughness on the surface spreading of an aqueous nanodrop. *Faraday Discussions* **2010,** *146*, 66-77.
16. Berendsen, H. J. C.; Grigera, J. R.; Straatsma, T. P. The Missing Term In Effective Pair Potentials. *J. Phys. Chem.* **1987,** *91* (24), 6269-6271.
17. Plimpton, S. Fast Parallel Algorithms for Short-Range Molecular Dynamics. *J.*

Comput. Phys. **1995,** *117* (1).

18. de Ruijter, M. J.; Blake, T. D.; De Connick, J. Dynamic Wetting Studied by Molecular Modeling Simulations of Droplet Spreading. *Langmuir* **1999,** *15* (22), 7836-7847.
19. Humphrey, W.; Dalke, A.; Schulten, K. VMD - Visual Molecular Dynamics. *J. Molec. Graphics* **1996,** *14*, 33-38.
20. Moore, T. A.; Schroeder, D. V. A different approach to introducing statistical mechanics. *Am. J. Phys.* **1997,** *65* (1), 26-36.

Appendix A

LAMMPS Input File

```
# LAMMPS C++ molecule water drop on graphene plate

units           real
processors      1 1 1
boundary        p p p
neighbor        2.0 bin
atom_style      full

pair_style      lj/cut/coul/long 14.0
pair_modify     mix arithmetic
kspace_style    pppm 1.0E-6
bond_style      harmonic
angle_style     harmonic

read_data       lammps_GRA
group           water type 1 2
fix             1 water shake 0.000001 500 0 b 1 a 1
velocity    water create 300.0 2358 dist gaussian
```

```
group           graphine type 3
fix             2 graphine setforce 0.0 0.0 0.0
fix             3 water nvt 300.0 300.0 100.
neigh_modify  exclude group graphine graphine

timestep    1.0
thermo      1000
restart     200000      sio2.dump

dump        1 all atom 50000 dump.all
dump        2 water atom 1000 dump.water
run             400000
```

LAMMPS Data File

```
#LAMMPS data file for groups on graphene
11376 atoms
4000 bonds
2000 angles
0 dihedrals
0 impropers

3 atom types
1 bond types
```

1 angle types

0.000000000 117.888000 xlo xhi

0.000000000 119.109700 ylo yhi

0.000000000 300.000000 zlo zhi

Masses

1 15.9994

2 1.00797

3 12.011

Pair Coeffs

1 0.1552976020 3.1655200879

2 0.0000000000 0.0000000000

3 0.0231060600 3.2144799121

Bond Coeffs

1 0. 1.

Angle Coeffs

1 0.00 109.47

Atoms

#(Atom No. Molecule No. Atom Type. Partial Charge X Y Z)

1 1 3 0 0 0 0 …

5376 1 3 0 67.54 118.4008 0

5377 2 1 -0.8476 83.227380 72.295855 7.40030 …

11376 2001 2 0.4238 65.496380 52.676955 14.57930

Bonds

1 1 5377 5378 …

4000 1 11374 11376

Angles

1 1 5378 5377 5379 …

2000 1 11375 11374 11376

Vita

John Andre Ritchie was born on June 17, 1964, in Mobile, Alabama and is a citizen of the United States of America. He graduated from John S. Shaw High School, Mobile, Alabama in 1982. He received his Bachelor of Science in Chemistry from Kennesaw University, Kennesaw, Georgia in 1995 and subsequently has worked as a chemist in the specialty chemicals industry where he is currently employed with Rochester Midland Corporation as their representative in Virginia.